THE FASTGAS DETECTOR

J.E.Bateman, R. Dalgliesh, D.M.Duxbury, S.A.Holt, D. McPhail,
A.S.Marsh, N.J.Rhodes, E.M.Schooneveld, E.J.Spill and R.Stephenson

Science and Technology Facilities Council, Rutherford Appleton Laboratory, Harwell
Science and Innovation Campus, Didcot, Oxfordshire, OX11 0QX, U.K.

20 October 2009

Abstract

The development and testing of the FastGas neutron detector is described. Based on a Microstrip Gas Chamber the aim of the project was to produce a high counting rate detector capable of replacing the existing ^{3}He tubes for specular reflectometry, currently in use on the ISIS reflectometer instruments. The detector system is described together with results of neutron beam tests carried out at the ISIS spallation neutron source.

1. Introduction

Following the successful testing of a 2D imaging detector based on the gas microstrip detector (MSGC) technology [1] on the ROTAX beamline at ISIS [2], it became clear that this technology could offer significant detection capabilities for further experiments on ISIS beamlines. The CRISP reflectometer [3,4] is an instrument which is primarily used for time of flight neutron reflection experiments from surfaces and interfaces. In its specular reflection mode the instrument uses a single, one inch diameter wire detector filled with 3.5 bars of neutron sensitive ^{3}He, which is used to measure the intensity of the reflected neutron beam.

The FastGas project was a development programme aimed at demonstrating that MSGC technology could successfully be applied to the field of neutron detection in order to replace the ^{3}He tubes, the count rate performance of which has been shown to deteriorate quite rapidly at relatively modest neutron fluxes. Based on the same ^{3}He neutron converter with added quencher, this technology can offer a high rate capability with good timing resolution and low gamma sensitivity at high neutron detection efficiencies in the 1-10Å wavelength range.

The CRISP instrument is also used to measure off specular reflectivity with a linear position sensitive fibre coded ZnS:Ag/^{6}LiF scintillation detector. This scintillation detector is more robust than the ^{3}He tube and has a similar rate capability, but is limited to a position resolution of 1.2mm. A further development to produce a 1D ^{3}He gas based detector which will deliver a position resolution of 0.5mm is currently underway (OSMOND), but is beyond the scope of this report. However it will be necessary to operate such a detector with 2-4 bars of dense quencher (CO_2 or CF_4) in order to keep the proton range small enough to achieve this. Therefore as part of the FastGas development programme we intended to demonstrate that it was possible to operate these types of device with a large fraction of CO_2 or CF_4 as the quench gas, in a pulsed neutron source, for reflectometry applications.

2. FastGas Detector Design

The FastGas MSGC glass plates are of the same basic design as those described previously [5]. The MSGC pattern is etched into 0.5μm chromium and comprises of 10μm wide anodes interleaved with 90μm wide cathodes on a 300μm pitch. The plates are produced at IMT [6] on Schott S8900 conducting glass [7]. The glass plate consists of eight sections, each of which has 10 anodes connected together with an active length of 60mm, and can be seen in figure 1(a). The plates themselves are glued to a printed circuit board (PCB) and are ultrasonically wire bonded to pads on the PCB. The cathodes are biased via a filter network on the reverse of the PCB and the anodes are tracked to a 15 way D connector. The PCB is then mated to a 15 way vacuum feed-through flange at one end and supported on spacers at the other end to keep the plate level. This flange is welded into the stainless steel detector vessel along with two high voltage feed-throughs. An aluminium window is bolted to the vessel and the gas seal is made by using a Garlock

seal [8]. The drift plane is mounted on the inside of this window and is insulated from the window by using ceramic spacers. A high voltage connection is made to the drift plane by means of a spring loaded contact and the drift depth is defined as 25mm. A gas inlet pipe is also welded into the vessel and is sealed off with a swagelock valve [9] thus enabling the vessel to be pressurised. The vessel has been designed and pressure tested to operate at 14 bar gauge pressure and can be seen in figure 1 (b).

The signals from each group of anodes are input to a 16 channel charge preamp [10] (eight channels of which are redundant) which is mounted on the reverse of the 15 way D feed-through in a custom built external housing. The differential output pulse is then sent via a 15m cable to a signal converter unit, which in turn feeds the signals to an eight channel NIM based discriminator. From here the signals can then be fed to the ISIS Data Acquisition Electronics system (DAE) [11]. Alternatively, the fast signals from the signal converter unit can be stretched in time (by a simple RC circuit) before being amplified by a standard Ortec 575 post-amplifier, where they can then be fed to a Pulse Height Analyser (PHA) to give the corresponding pulse height spectrum. Each section of the plate can be operated independently, albeit with the same operating characteristics (and the same biasing supplies), or all eight sections can be summed together externally giving an active detector area of 60mm by 24mm.

3. System Performance

The performance of the FastGas detector was characterised using two sets of facilities. The basic characterisation and long-term stability was measured using a moderated ^{241}Am:Be source which was capable of inducing a counting rate of ~140Hz in a single section of the detector – adequate for these purposes. For high rate tests, exposures were arranged on various ISIS beam lines (ROTAX [12], CRISP, SURF [13]) as limited time slots became available.

As one of the putative applications of the FastGas detector is to replace the 1 inch diameter single wire counters installed on the CRISP reflectometer, the detector was designed to operate with a filling of 10 bar ^{3}He to achieve a nominal neutron stopping efficiency of 87% at a neutron wavelength of 1Å. Two quenchers are used: CF_4 and CO_2 each at 4 bar pressure.

3.1 Basic Properties

Typical pulse height spectra obtained from a single section of the detector are shown in figures 2 and 3, with CF_4 and CO_2 as quencher respectively at typical operating conditions. In both cases a clear peak is observed corresponding to the full deposit of the 765keV energy deposit from the Q of the detection nuclear reaction. The maximum sustainable drift voltage for the two cases was different, but this does not have a large effect on the gain (see figure 8). From these peaks, pulse gain curves can be calculated as seen in figure 4.

Some points are evident from these results:

- Higher bias voltages are required with the CF_4 quencher. However, this is not a problem as its high dielectric strength keeps the detector stable and permits higher gains than the CO_2 quencher.

- CF_4 produces a much cleaner pulse height spectrum. This is simply because of the factor of $\times 2$ density advantage of CF_4 over CO_2 which restricts the leakage of the event signal out of the fiducial collecting volume caused by the escape of the 570keV proton (range ~1.7mm in 4 bar CO_2).

- The gains obtainable are low by the standards of X-ray detectors. This is unimportant because the initial charge signal from the ^{3}He (n,α) reaction is $\times 100$ greater than the typical X-ray signal so that a gain of $\times 10$ is adequate to bring the charge signal into the comfortable working range of 2-3$\times 10^5$ electrons. It is only required to obtain adequate gain to ensure that the temporal pulse formation is kept stable and short. A gain of $\times 10$ seems more than adequate to assure this with the small dimensions of the MSGC section.

The full-energy peak was used to measure the gain uniformity of the MSGC plate as a whole. Figure 5 shows the result. There are two outliers to the typical 1-2% uniformity observed in MSGC gains but they are not severe and don't detract from the possibility of using the dramatically improved spatial resolution relative to 1 inch diameter tubes by instrumenting each of the 8 plate sections.

An option available with the FastGas detector is to use adjacent sections to veto the events where serious proton leakage out of the section occurs. Figure 6 shows the effect on the pulse height spectrum of vetoing events in a section with triggers from its neighbours in a CO_2 gas filling (trigger threshold set to 200keV). Almost all the small pulses disappear (MSGC plate and window end effects are inevitably still present). The corresponding process shows less benefit in the case of a CF_4 filling, figure 7, but the vetoing does remove some of the smaller events from the pulse height spectrum. This process costs some detection efficiency and would in general not be used; however in a high-gamma background environment it may well be very useful.

At the high pressures required for efficient operation, the drift field must be sufficient to ensure effective charge collection onto the MSGC anodes. Two physical processes affect this. First, the electron clouds spread by diffusion during the drift process with the possibility of degrading the pulse height spectrum. At the drift potential values used ($V_d > 10$kV) it turns out that diffusion spreading is much less than the proton range which dominates. In fact results on diffusion in 4 bar CO_2 [14] indicate an RMS spread of <100μm in the FastGas drift field (the 10 bar of ^{3}He has little effect on the electron temperature). The second effect can be caused by electron attachment during the drift process, leading to highly distorted pulse height spectra and loss of signal.

A simple measurement can confirm that neither of these two effects is seriously present. It has been shown elsewhere [15] that the gain of an MSGC with a drift section and perfect charge collection is dependent on the parameter $V_d + \alpha V_b$ (where V_d is the drift voltage and V_b is the bias voltage of the MSGC plate) so that plotting V_b versus V_d at constant gain should give a straight line if no drift loss processes are significant. Figure 8 shows such a plot with a reasonable straight line fit. This, together with the excellent pulse height spectra, gives total confidence in the operation of the detector. Figure 8 shows that $\alpha = 4.1 \times 10^{-3}$, making the gain fairly insensitive to the drift potential.

3.2 Operational Stability

The stability criteria required of the detector fall into two categories – short-term (approximately the duration of experimental procedures on ISIS) and long-term (defining the aging characteristics of the device and reliability).

The short-term stability was assessed by counting the ^{241}Am:Be source for several days in time bins of 300 seconds with a counting threshold of 200keV (which captures most of the converted events) The filling was ^{3}He + CF_4. Figure 9 shows the output of a multi-channel scaler over a period of 3.47 days. The SD of the rate is 0.28%, very little more than the Poisson error of 0.25%. Re-binning of the data into 3000 second bins yielded a standard deviation of 0.15%. This falls comfortably within the specification of 0.5% count stability over a 48 hour period.

Early experience with the detector gave excellent results in the short term but over a period of a few weeks a serious degradation of the properties set in, indicating that contamination of the gas was a problem. A program of improvements was undertaken of which the main one was the replacement of all insulating materials in the detector volume with ceramic. This allowed an enhanced bake-out temperature of 105°C. Long-term tests were undertaken on the improved detector with a filling of ^{3}He and CO_2. After some initial transient instability the detector was tracked over a period of 5×10^4 minutes (35 days). The gain and the counting rates above various thresholds are shown in figure 10.

Considering the data with an LLD of 200keV (the most likely value) we see a systematic rise in the counting rate of 0.053%/day with a standard error of 0.7% over the month. The rates at all LLD values show a similar performance. The counting rate is clearly not sensitive to the gain which shows much more dramatic variation over the period. When the gain is plotted alongside the plate current, figure 11, the anti-correlation is obvious. Since the plate current (I_c) is proportional to temperature (over such a small range) it can be used as a thermometer. Calibration against an external thermometer gives $dI_c/dT = 0.237\mu A/C$. Making a plot of the gain (G) against I_c from figure 11 reveals $dG/dI_c \sim -0.5/\mu A$ which combined with dI_c/dT gives $1/G(dG/dT) = 2.2\%/C$. Given that the detector box is of fixed volume the usual modality of temperature variation (change of the mean free path) does not apply and this high value is almost certainly associated with desorption of contaminants from the counter materials.

The temperature dependence of the gain can be normalised out of the gain curve of figure 11, by normalising the measured gain to a standard plate current (i.e. temperature). The data of figure 11 provides the calibration of gain versus plate current. Figure 12 shows this result, including the initial unstable period, with the gain showing an asymptotic approach to a stable value with a time constant of 30 days. This again points to a 'clean-up' of the gas over time.

It was noticed after a prolonged period (several months) that the gain-temperature coefficient noted above was reducing markedly. This tends to reinforce the conclusion that the early instabilities are the result of chemi-sorption processes between the gas and the vessel structure which eventually saturate and stabilise.

3.3 Gamma Sensitivity

The gamma sensitivity of the detector has been measured by using a ^{60}Co gamma source (1.3MeV). Figure 13 shows the spectra obtained both with and without the gamma source present in a low neutron background region of the source laboratory for an acquisition period of 25000 seconds. The peak seen in this data cannot be attributed to the neutron source or to the cosmic ray background and is therefore suspected to be due to activated material either in the vessel or the vessel itself. Gamma sensitivity values of 3.8×10^{-4}, 2.5×10^{-5}, 1.1×10^{-5}, and 7.9×10^{-6} were obtained for LLD settings of 100, 200, 300 and 400keV respectively.

3.4 High rate tests

With the vessel filled with a ^{3}He:CO_2 gas mixture, FastGas was installed on the CRISP reflectometer with the electrodes of the MSGC running vertically. The CRISP beamline has a pair of horizontal slits situated before the sample position which open up vertically thereby giving us the ability to alter the neutron flux hitting the detector. The signals from the detector were fed to the DAE, via a discriminator with the LLD set to 200keV. Figure 14 shows the counting rate from FastGas as the slit size is increased from 0.2mm to 8.0mm, as measured on an external scaler (Tektronix DC503 – 100MHz). At each slit setting the counting rate on the scaler was measured from a single section then the sum of 2 sections, then the sum of 3, contiguously up to the sum of 8 sections. For clarity only the curves from a single (typical) section and 7 sections are shown (7 sections match most closely the 25mm aperture of the standard ^{3}He tube). The count rate per frame as measured by the DAE for a single section is shown multiplied by a factor of 50 for comparison with the scaler data. (In normal operation ISIS operates at 50 frames per second). It is noted that the response of the DAE and the scaler are identical up to the maximum rate in this section of 150kHz. As sections are added, the scaler rate scales appropriately – as seen from the ratio curve in figure 14 indicating that the neutron flux is relatively uniform over the aperture. However, there is a consistent deficit of about 5% (see figure 14) which probably reflects the slight over-counting which occurs in any given section due to occasional charge sharing between sections, consequent on the proton range. It is also seen from the same curve that some rate deterioration of the capture efficiency starts to show above ~400kHz.

The corresponding neutron Time Of Flight (TOF) spectra are shown in figure 15 for each slit setting, from a single section of FastGas. Each TOF spectrum was 10000 frames in length.

In assessing the rate performance of pulse counting systems driven by a stream of pulses which are randomly distributed in time, it is found that a simple deadtime relation relates the output (or capture) rate N_o of the system to the incident rate N_i over the useful portion of the dynamic range.

$$N_o^{-1} = N_i^{-1} + \tau \qquad (1)$$

Where τ is the deadtime of the system – a parameter which may be fixed electronically or (if uncontrolled) is generally a function of the spectrum of incident pulse heights as well as the properties of the discriminator circuit. Simple manipulation of this formula reveals two useful properties: (1) in the case of pulses passed sequentially through several circuits the overall performance is just given by equation (1) with τ now simply equal to the sum of the deadtimes of each circuit; (2) in the case of *n* pulse streams "ORed" together digitally the same formula holds with τ now replaced by τ/n.

It was possible to compare the performance of FastGas to the standard ^{3}He tube simply by removing FastGas from the beam as the tube was already mounted in position, albeit further from the sample position which thus time-shifts the neutron TOF spectrum. Figure 16 shows the ^{3}He tube TOF spectra as the slit size is increased from 0.2 to 1.0mm; again the spectrum were also collected for 10000 frames each. Previous experience has shown that the performance of the tube starts to deteriorate with the slit opening greater than 0.5mm. This can be seen in figure 17 where the TOF spectra are normalised by the smallest slit setting and a large drop in counts is observed around 7500μs at the peak in the Maxwellian. The cause of this drop in performance is due to the long ion collection time of the tube. If the same normalisation is applied to the FastGas data from figure 14, no noticeable drop in performance is observed - figure 18. If care is taken to smooth the data in the 1mm/0.2mm in figure 17, then it is possible to estimate the deadtime of the ^{3}He tube from it. (The method for doing this is illustrated below with the statistically superior FastGas data). The deadtime of the ^{3}He tube evaluates to 6.16μs.

FastGas was then put back in the beam in an attempt to observe the point at which the detector performance began to sag with neutron flux. In order to remove any memory limitations of the DAE from contributing to the observed detector dead time, the time of flight range that the DAE collected data was reduced to between 5000 and 7300μs. Seven sections were summed together and fed to the DAE and the slits were increased from 0.5 to 8mm. The normalised TOF spectra can be seen in figure 19. Figure 19 clearly shows that the performance of FastGas would appear to be deteriorating at a slit setting of 7mm and above, as indicated by the dip around 6500μs. This spectral distortion can be employed as a means to assess the overall deadtime of the whole system by using equation (1) in the form:

$$N_o/N_i = 1 - N_o\tau \qquad (2)$$

If we assume that the counting system is operating in the linear region at the smallest slit aperture (0.5mm) the denominator of the ratio plots of figure 19 can be assumed to be proportional to N_i, i.e. the ordinate is $N_o/\alpha N_i$. Figure 20 shows that the straight lines predicted by equation (2) do in fact result when the ratios of figure 20 are plotted against the instantaneous rate for the corresponding TOF channel. As the slit size of the numerator decreases so does the measured value of τ – clearly it goes to zero when the slits are identical. The correct value of τ is simply obtained by plotting the measured values against $1/\alpha$ and taking the value when $1/\alpha = 0$. Figure 21 shows a simple linear dependence giving confidence in the method. In this way we find $\tau = 0.312\mu s$.

With the data in hand it is possible to check the consistency of the counter rate performance as measured by the DAE (as above) and into the fast scaler. We can use the observed global scaler rates to estimate the rate corresponding to a TOF channel. (We note that the scaler rate contains 50 frames of 20000 channels and figure 15 allows us to show that the mean rate in the 5000 - 7300µs window is 2.52 times the global mean). In figure 22 the DAE capture rate is plotted against the channel rate estimated from the scaler. In order to make the data fit the DAE deadtime of 0.312µs a deadtime of 0.184µs must be assumed for the 7-section counter-scaler system. It is known from x-ray versions of this type of detector, with the same charge gain, preamplifier and roughly the same time-charge distribution [16], that the deadtime of the counter-discriminator system is ~350ns. Which in the paralleled system should give 350/7 = 50ns plus the 50ns pulse width of the discriminators and 10ns from the scaler giving 110ns. This is somewhat shy of the 184ns fitted and the precise source of the discrepancy has not been identified.

The specific DAE contribution to the deadtime can be estimated at 312 – 184 = 124ns. Thus it can be concluded that in this 7-section configuration the counter and data collection deadtimes are well matched.

Because of the way the data is collected in the present tests, the above results do not represent the ultimate rate capabilities of the FastGas detector. In x-ray tests of a similar design using the same electronics and virtually identical pulse sizes (~2.5 x10^5 electrons) a single strip (i.e. one tenth of the number paralled up in a FastGas section) yields a deadtime curve similar to that of figure 22 with a deadtime of 350ns [16]. In the present tests the signals from 10 channels are bussed on the detector surface and the digital outputs from 7 sections bussed together before insertion into a single DAE channel. The front-end deadtime is largely determined by the width of the RC-shaped analogue pulse from the amplifier (~150ns FWHM). Bussing at the digital output stage saves some time – which explains the marginally faster response (184ns) estimated for the scaler data capture. The limitations of the front-end chain are easily overcome by inserting the 7 section channels into separate DAE channels and summing off-line. This would give an effective deadtime of the order of 350/7, i.e. ~50ns (plus perhaps a further 20ns from the DAE). Any further advance in the rate capability would require the use of smaller sections on the plate and more electronic channels – a consequence of which would be a degraded pulse height spectrum (not necessarily a concern) due to the proton range.

3.5 Detection Efficiency

The theoretical neutron detection efficiency for FastGas with 10 bars of ^{3}He and a 25mm drift depth should be 86.7% at 1Å [17], increasing to ~100% from 2Å upwards. A cross-calibration of the detection efficiencies of the FastGas detector and the standard ^{3}He tube was not possible. This was mainly due to the two detectors being in radically different geometrical positions with respect to the neutron beam such that they would inevitably sample different parts of the beam structure, making a direct comparison impossible.

4. Application to Neutron Reflection Measurements

A ^{58}Ni standard was then placed in the beam in order to obtain reflection data. Figure 23 shows the TOF spectra obtained with both FastGas and the ^{3}He tube. The flight times have been corrected for the detector positions in this figure. The two data sets have been normalised for beam current, but the ^{3}He tube data was collected in a much shorter time interval thus explaining the low statistics data around 5000μs. The large difference between the two data sets below 5000μs is simply due to the fact that the ^{3}He tube is completely surrounded in B_4C shielding to remove the background events (which are clearly evident in the data set for FastGas). This data can be transformed to show the reflectivity as a function of momentum transfer Q, shown in figure 24, which again shows the data from FastGas and the ^{3}He tube. It is also evident from these figures that there is more neutron absorption/scattering at longer neutron wavelengths (flight times) in FastGas compared to the ^{3}He tube, due to the fact that the efficiency of the FastGas detector has saturated at close to 100% beyond 2Å while the lower efficiency of the ^{3}He tube is still rising.

5. Conclusions and future developments

The FastGas development programme has demonstrated that the MSGC technology can successfully be applied to high rate, high efficiency neutron detection for reflectometry applications on pulsed sources. The count rate performance of the detector as installed for this test has been shown to be 19.7 times greater (6.16μs/0.312μs) than that of a standard ^{3}He tube, whilst also offering good timing resolution and low gamma sensitivity at high neutron detection efficiencies in the 1-10Å wavelength range. With slight reorganisation of the data capture this figure of merit would improve by a further factor of approximately 10. Further substantial factors of rate improvement are potentially possible by further subdivision of the detector sections; however, this step would involve re-design of the basic GMSD plate pattern.

Since the program of improvements, alluded to in section 3.2, FastGas has only been run with a quencher of CO_2. This program is still ongoing and further measurements with a CF_4 quencher are scheduled to take place later this year along with extended high rate lifetime tests.

The ISIS second target station now has a further three reflectometer stations (INTER, OFFSPEC and POLREF), which at the time of writing are all undergoing scientific commissioning. It is strongly expected that the neutron flux on these experiments will be a factor of 10 to 20 times greater than that currently obtained on CRISP and that the science capabilities of these experiments will become detector limited. A modified design of the FastGas detector is seen as a potential replacement for the standard ^{3}He tube detectors for specular reflectivity measurements.

References

1. A. Oed, Nucl Instr & Meth **A261**(1988) 351
2. J.E. Bateman, G.E. Derbyshire, D.M. Duxbury, A.S. Marsh, N.J. Rhodes, E.M. Schooneveld, E.J. Spill and R. Stephenson, IEEE Trans. Nucl. Sci **52 (5)** (2005) 1693
3. J. Penfold, R.C. Ward and W.G. Williams, J. Phys. E: Sci. Instrum. **20** (1987) 1411
4. J. Penfold, Physica B **173** (1991) 1
5. A.D.Smith, J.E.Bateman, G.E.Derbyshire, D.M.Duxbury, J.Lipp, E.J.Spill and R.Stephenson, Nucl. Instr. and Meth. **A467-468** (2001) 1136
6. IMT, Greifensee, Switzerland
7. Schott Glass, Duryea, Pennsylvania, USA
8. Garlock (GB) Ltd, Premier Way, Lowfields Business Park, Elland, Wesy Yorkshire, UK, HX5 9HF
9. Swagelok, 29500 Solon Road, Solon, OH 44139 USA
10. J.E.Bateman, G.E.Derbyshire, G.Diakun, D.M.Duxbury, J.P.A.Fairclough, I.Harvey, W.I.Helsby, J.D.Lipp, A.S.Marsh, J.Salisbury, G.Sankar, E.J.Spill, R.Stephenson and N.J.Terrill, Nucl. Instr. and Meth. **A580** (2007) 1526
11. M. W. Johnson, S. P. Quinton, SNS data acquisition electronics (DAE), RAL-NDRP-8504
12. W. Schäfer, E. Jansen, R. Skowronek, G. Will, W. Kockelmann, W. Schmidt, H. Tietze-Jaensch, Nucl. Instr. and Method **A364** (1995) 179
13. D.G.Bucknall, J.Penfold, J.R.P.Webster, A.Zarbakhsh, R.M.Richardson, A.Rennie, J.S.Higgins, R.A.L.Jones et al. Proc. ICANS XIII, PSI Proceedings 95-02 Vol. 1 p123 (1995)
14. S. Bobkov, V. Cherniatin, B. Dolgoshein, G. Evgrafov, A. Kalinovsky, V. Kantserov, P. Nevsky, V. Sosnovtsev, A. Sumarokov and A. Selenov, CERN preprint EP/83-81 (1983)
15. J.E.Bateman, J.F.Connolly, G.E.Derbyshire, D.M.Duxbury, J.A.Mir, E.J.Spill, R.Stephenson, Nucl. Instr. and Meth. **A484** (2002) 384
16. J.E.Bateman, G.E.Derbyshire, G.Diakun, D.M.Duxbury, J.P.A.Fairclough, I.Harvey, W.I.Helsby, S-M. Mai, O.O. Mykhaylyk, G.Sankar, E.J.Spill, and R.Stephenson, IEEE Trans. Nucl. Sci., **55**, No.2, 729
17. J.E. Bateman, D.M. Duxbury, N.J. Rhodes, E.M. Schooneveld, and R. Stephenson, RAL-TR-2006-005

(a)   (b)
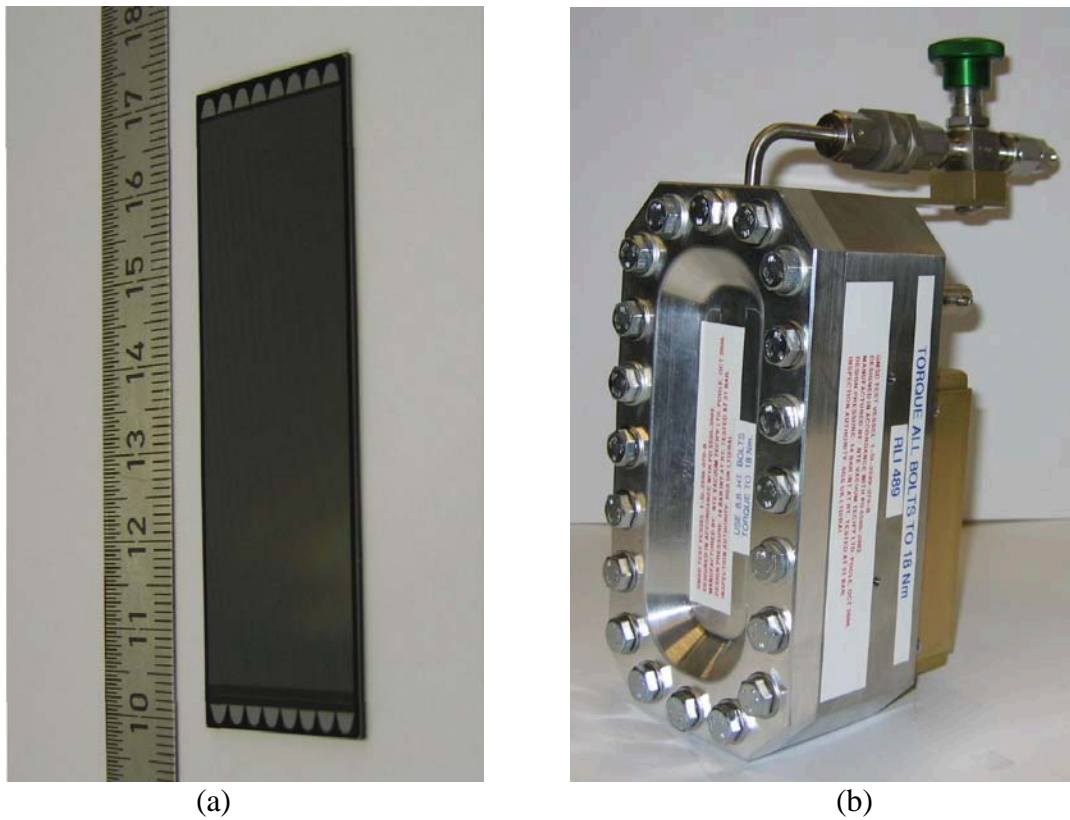
Figure 1: (a) shows the MSGC plate and (b) shows the assembled FastGas vessel
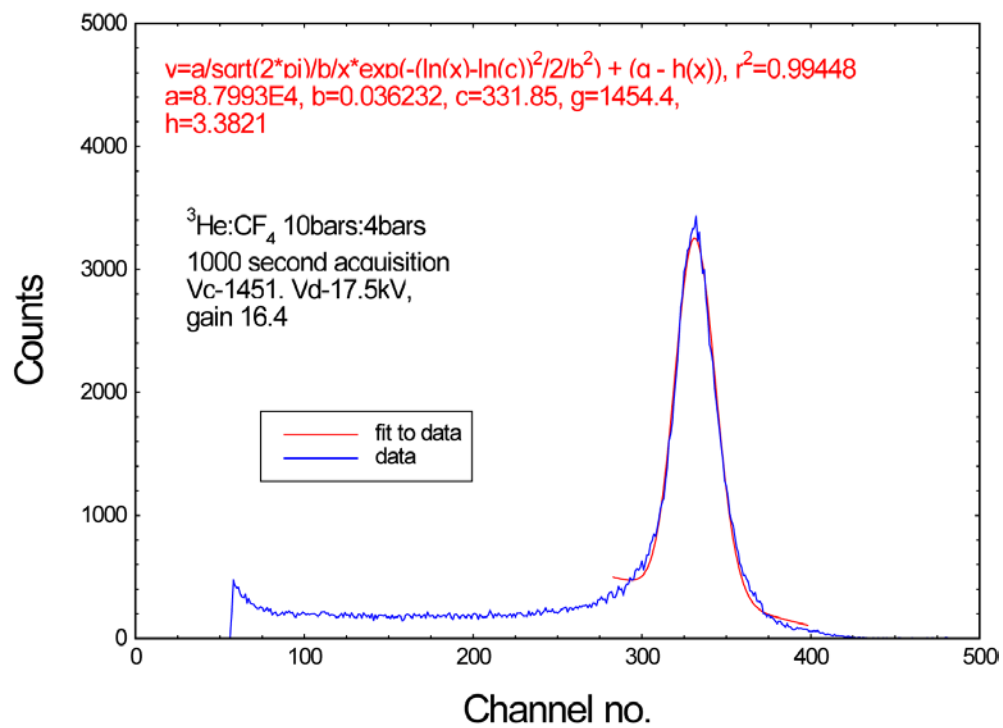
Figure 2: Pulse height distribution from ^{241}Am:Be source with CF_4 quencher

$$y=a/sqrt(2*pi)/b/x*exp(-(ln(x)-ln(c))^2)/2/b^2)) + (g - h(x)),$$
std-err:45.7 max dev:120.80. r^2=0.99655
a=4.0928E4, b=0.030764, c=248.79, g=1253.7,
h=4.1617

^{3}He:CO_2 10bars:4bars
1000 second acquisition
Vc-950. Vd-14kV
gain 10.62
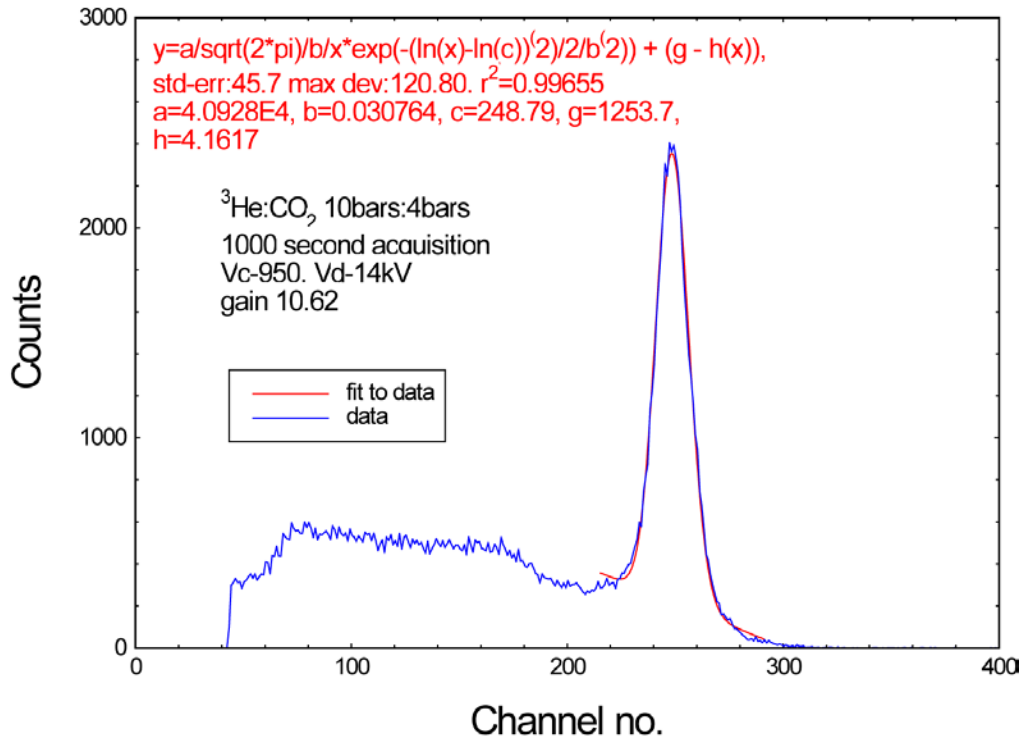
Figure 3: Pulse height distribution from ^{241}Am:Be source with CO_2 quencher
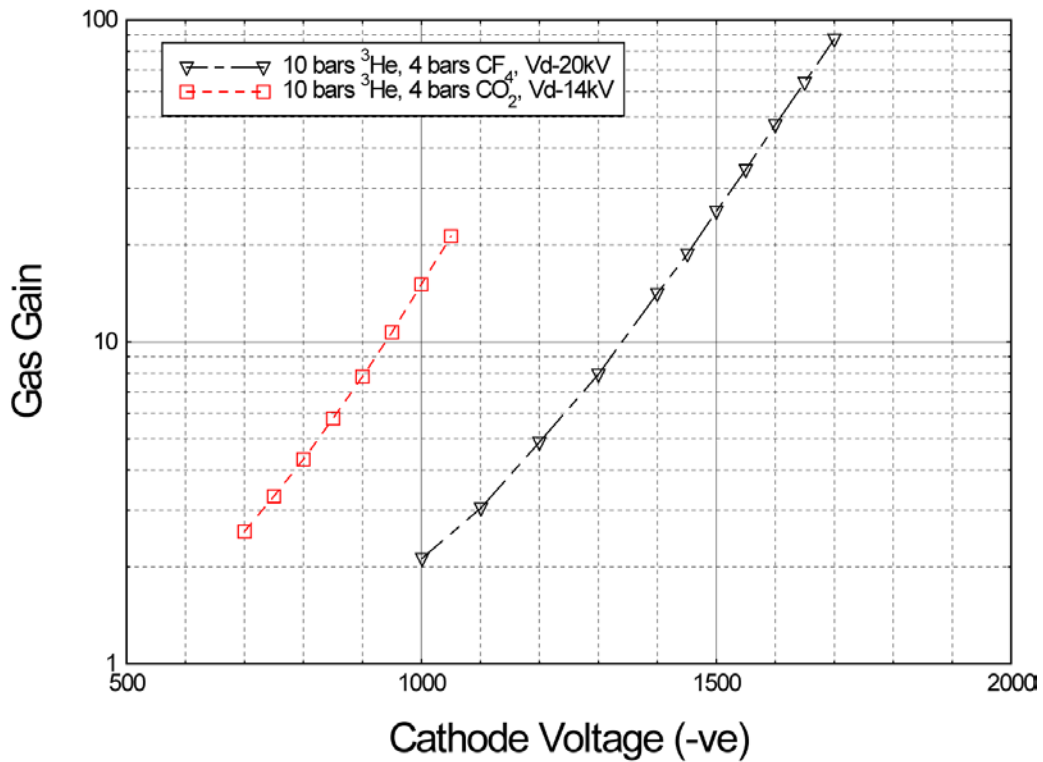
Figure 4: FastGas gain curves in ^{3}He:CF_4 and ^{3}He:CO_2 gas mixtures
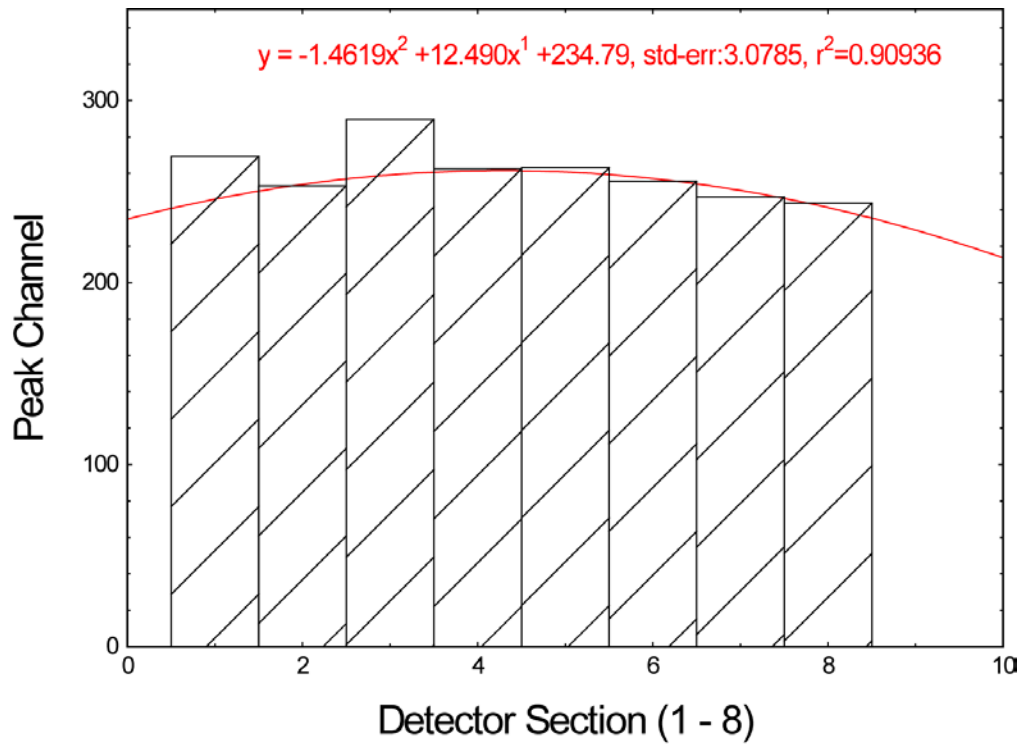
Figure 5: Plot showing the gain uniformity across the eight sections of the MSGC plate
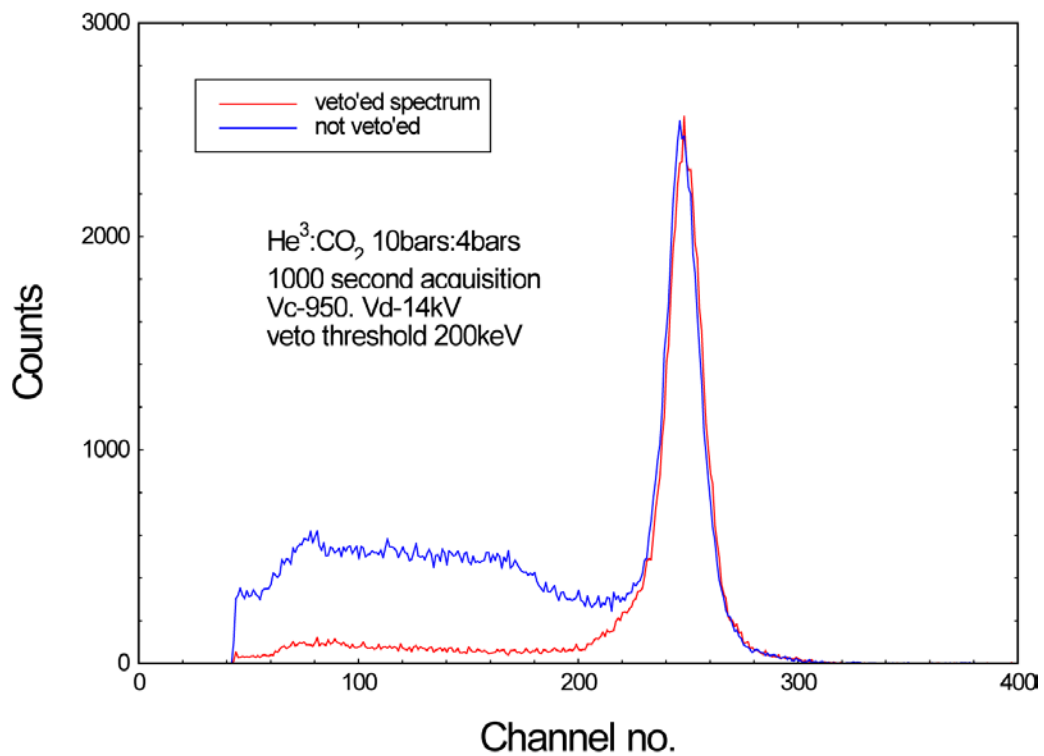
Figure 6: Pulse height distribution with and without veto with CO_2 quencher
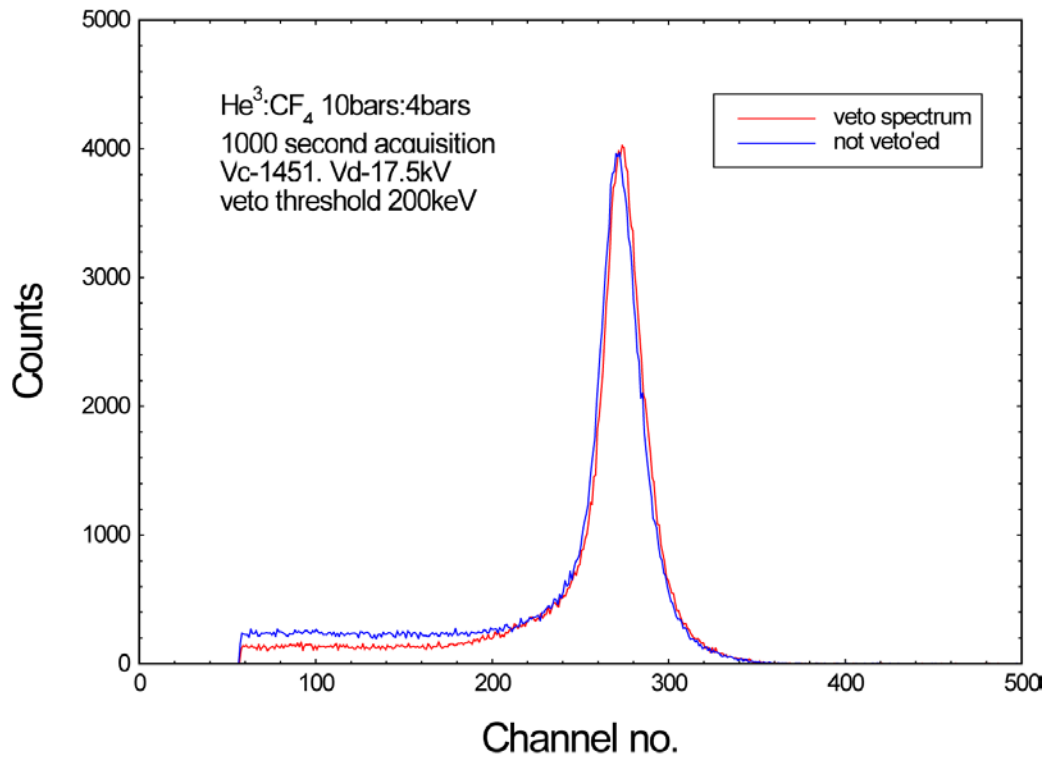
Figure 7: Pulse height distribution with and without veto with CF_4 quencher
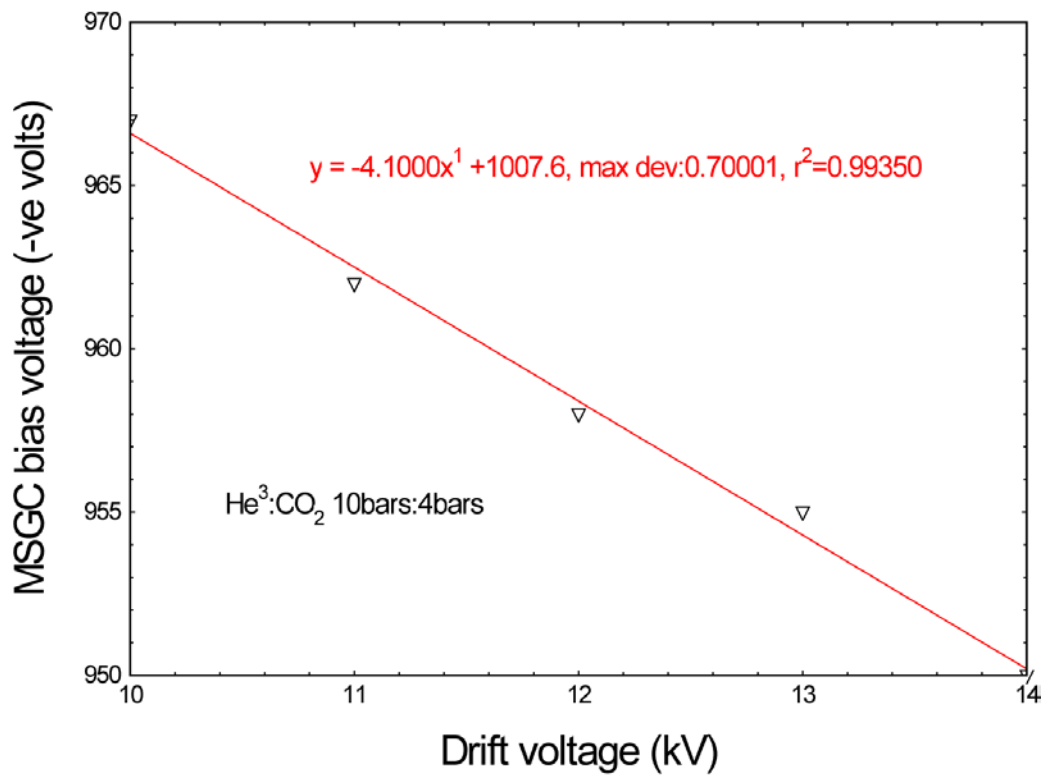
Figure 8: Plot of the drift voltage versus the cathode voltage for FastGas
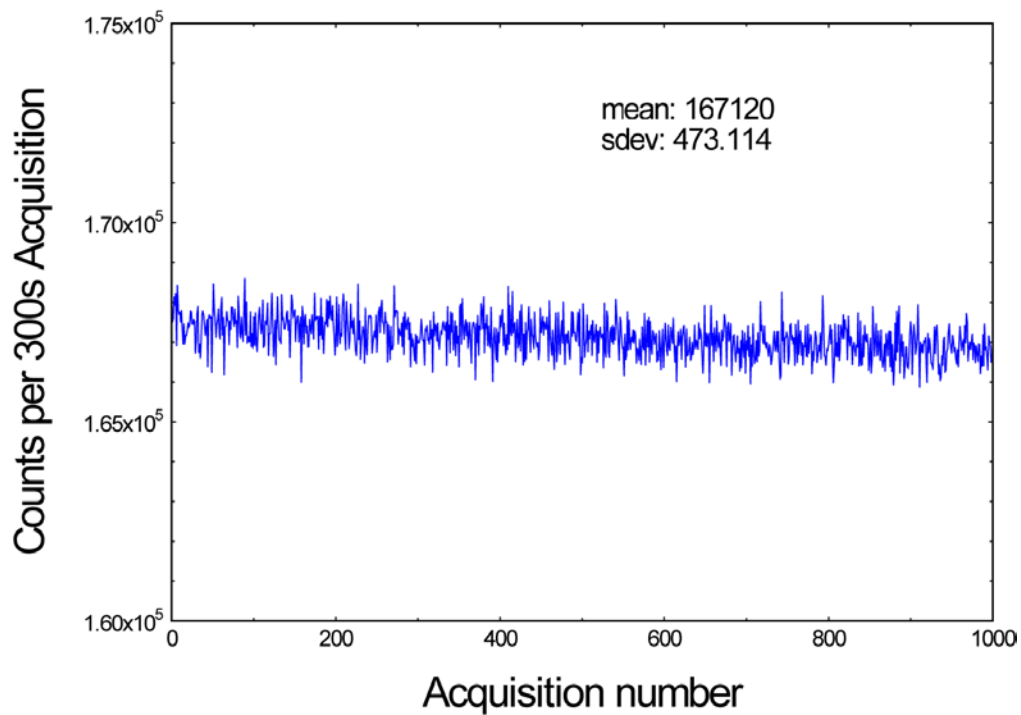
Figure 9: Count stability with 300 second time bins with the LLD setting at 200keV
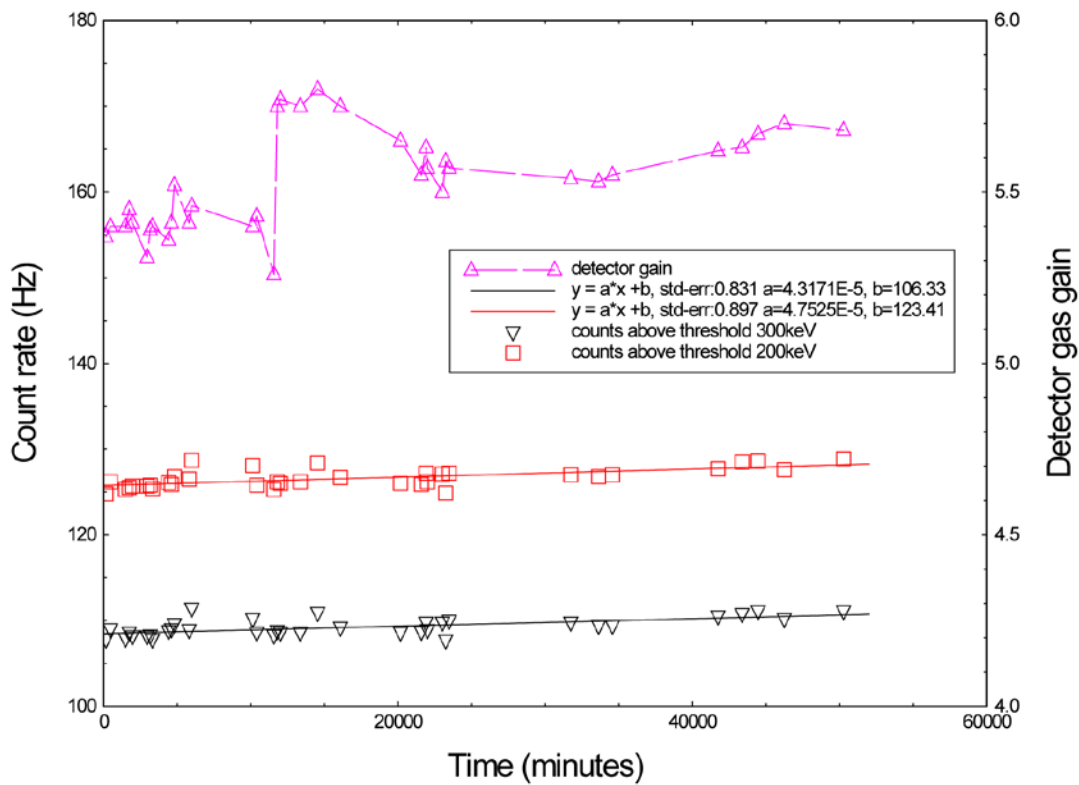
Figure 10: The gain and counting rate stability of FastGas over 35 days
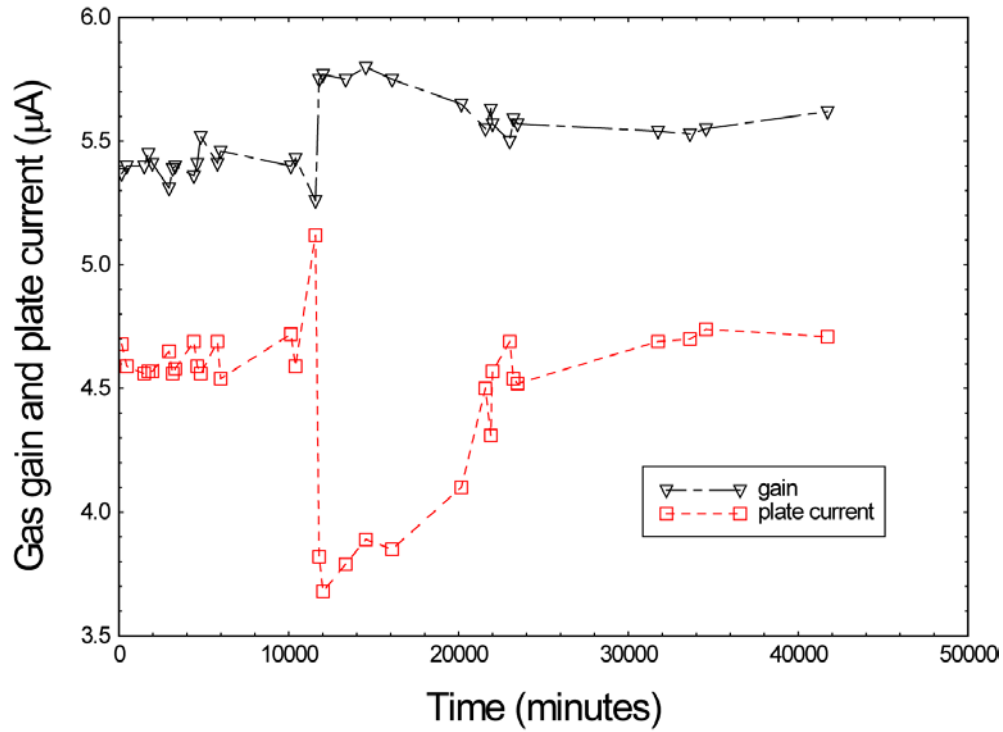
Figure 11: The gain and plate current variation of FastGas over 35 days
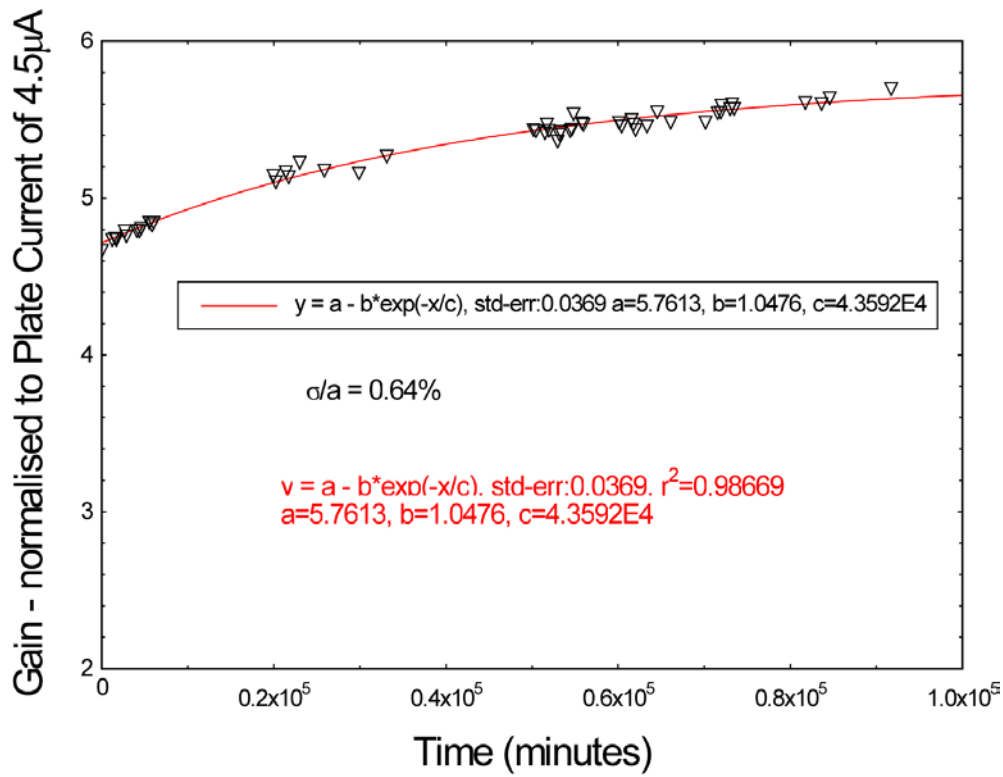
Figure 12: Gain variation data with temperature dependence removed
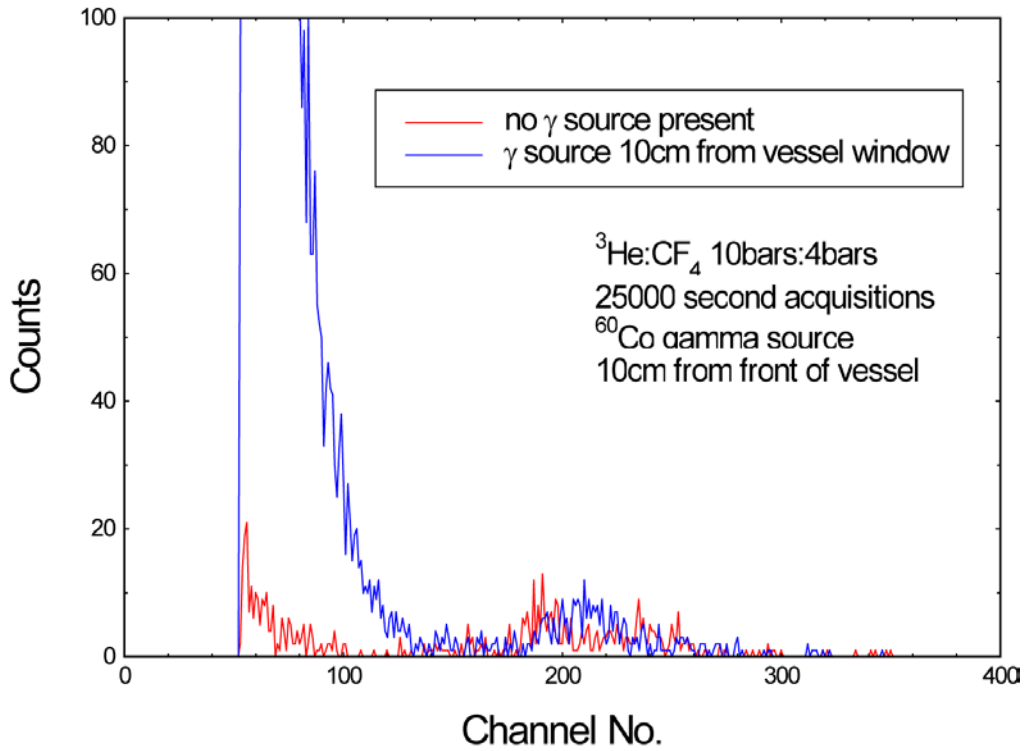
Figure 13: Pulse height spectra showing gamma sensitivity of FastGas detector
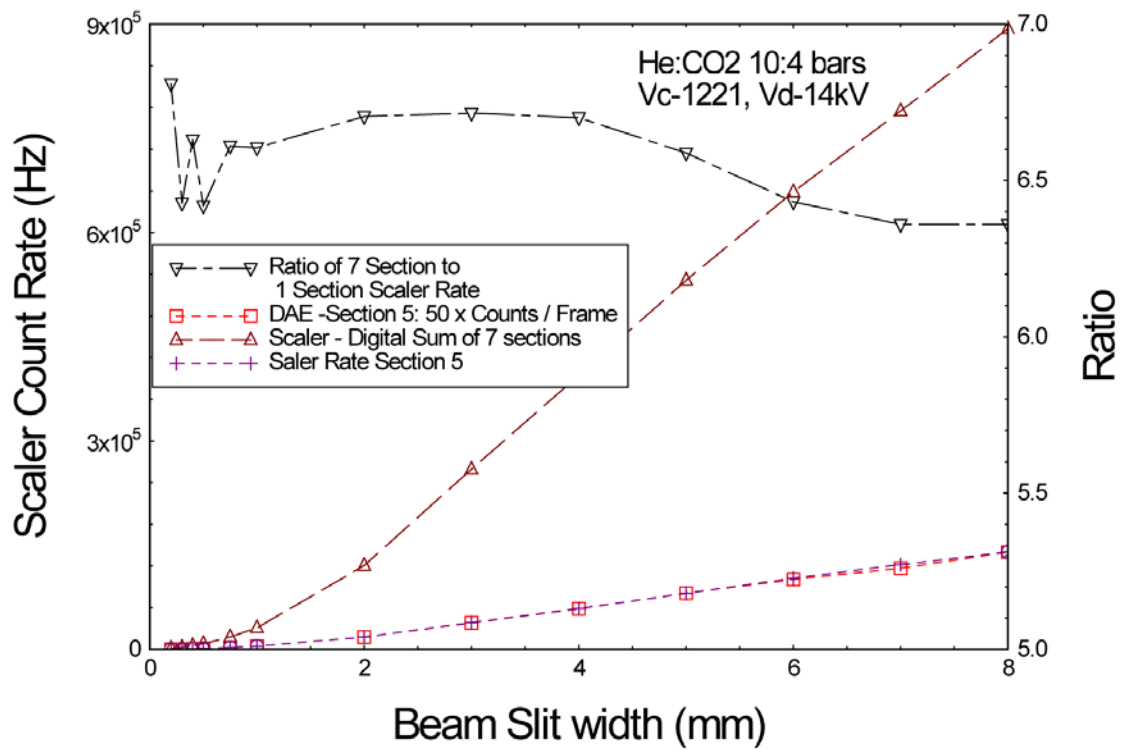
Figure 14: The counting rate from FastGas as the slit size is increased from 0.2 to 8.0mm
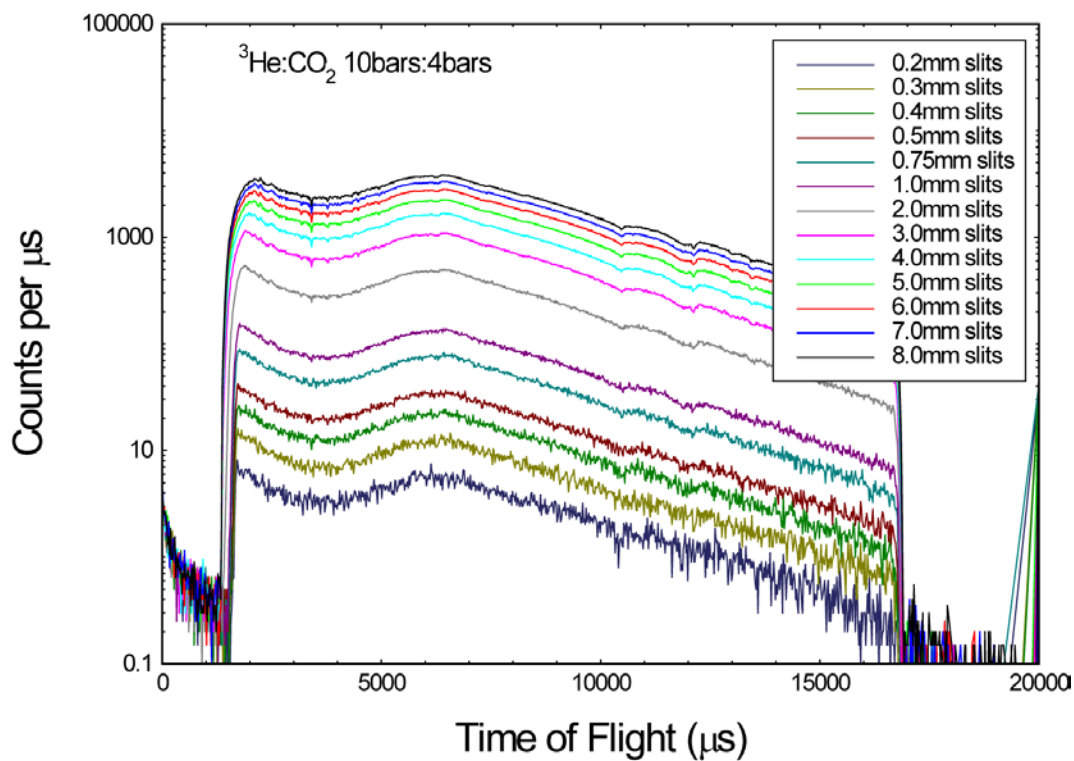
Figure 15: Corresponding TOF spectra from a single section of FastGas as slit size increased from 0.2 to 8.0mm
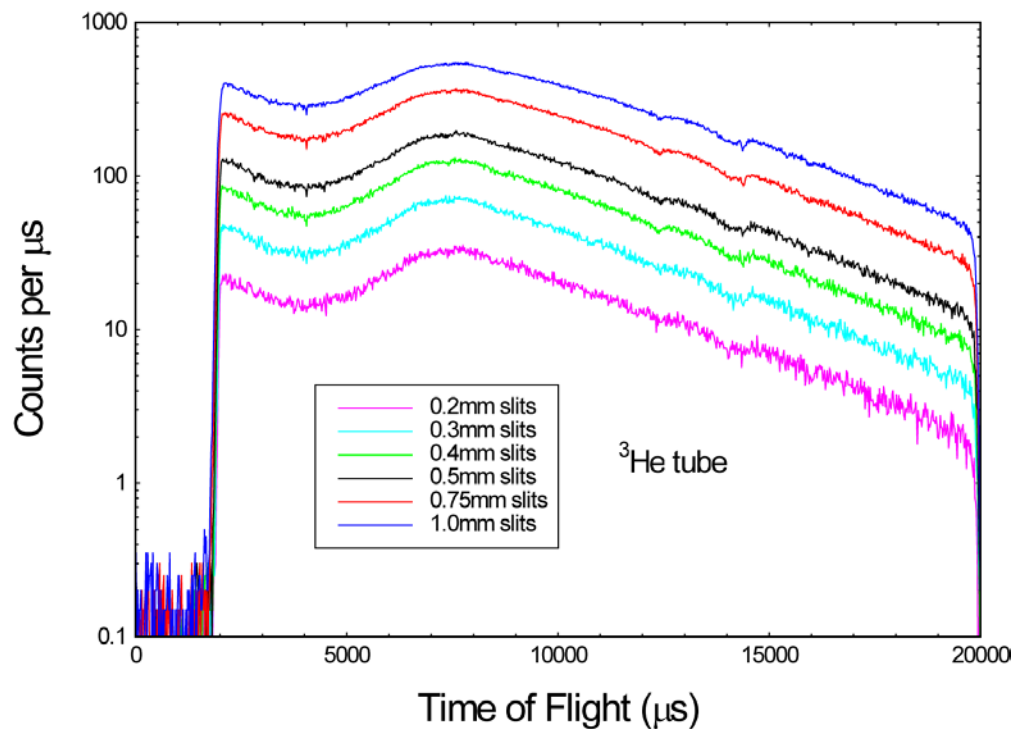
Figure 16: TOF spectra from a standard ^{3}He tube as slit size increases from 0.2 to 1.0mm
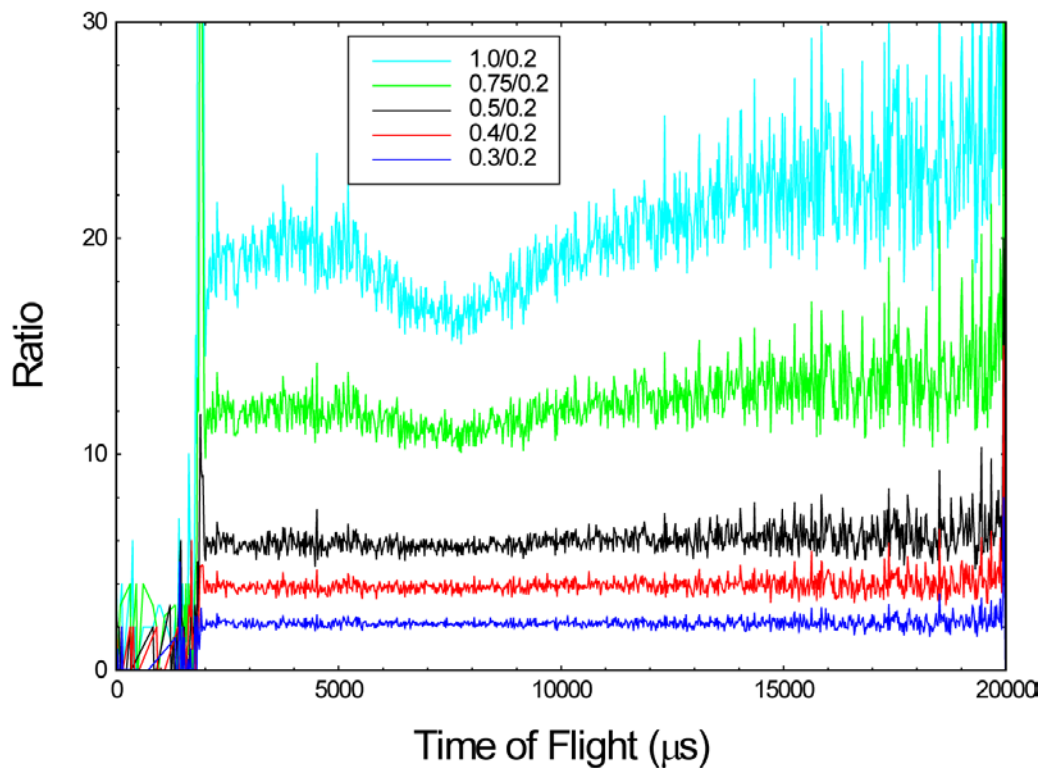
Figure 17: TOF spectra from figure 16, normalised to smallest slit setting
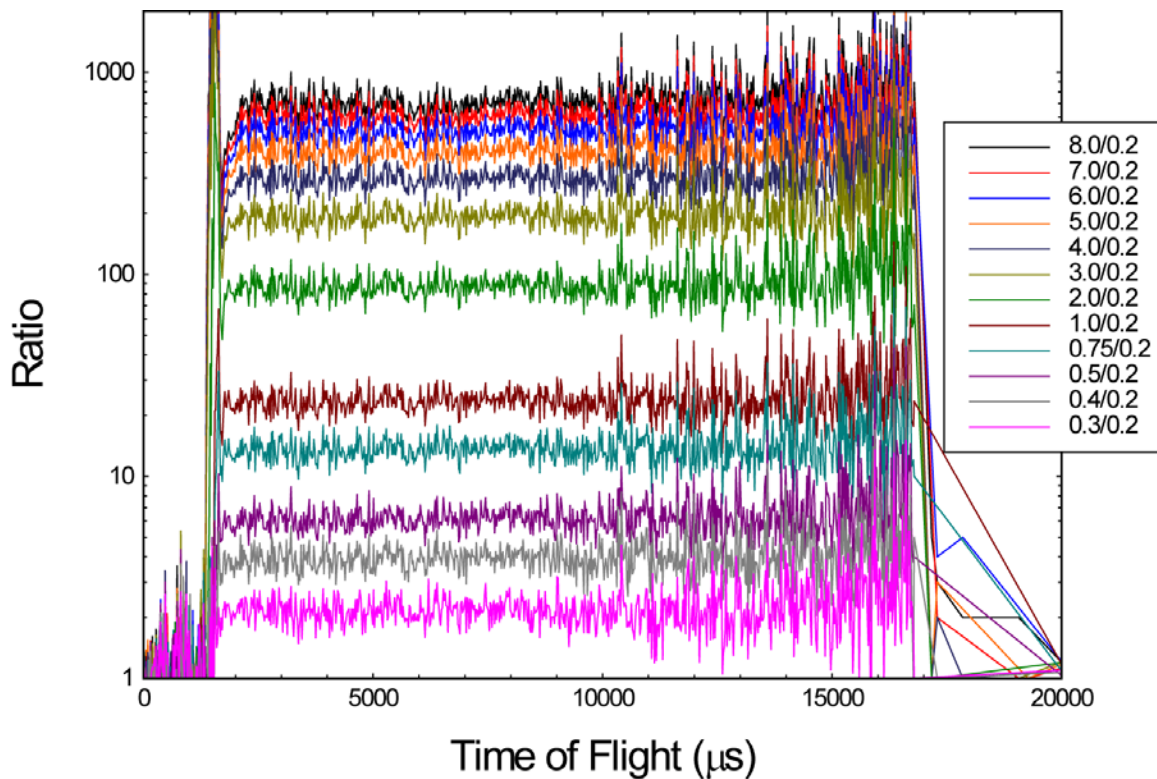
Figure 18: TOF spectra from figure 15, normalised to smallest slit setting
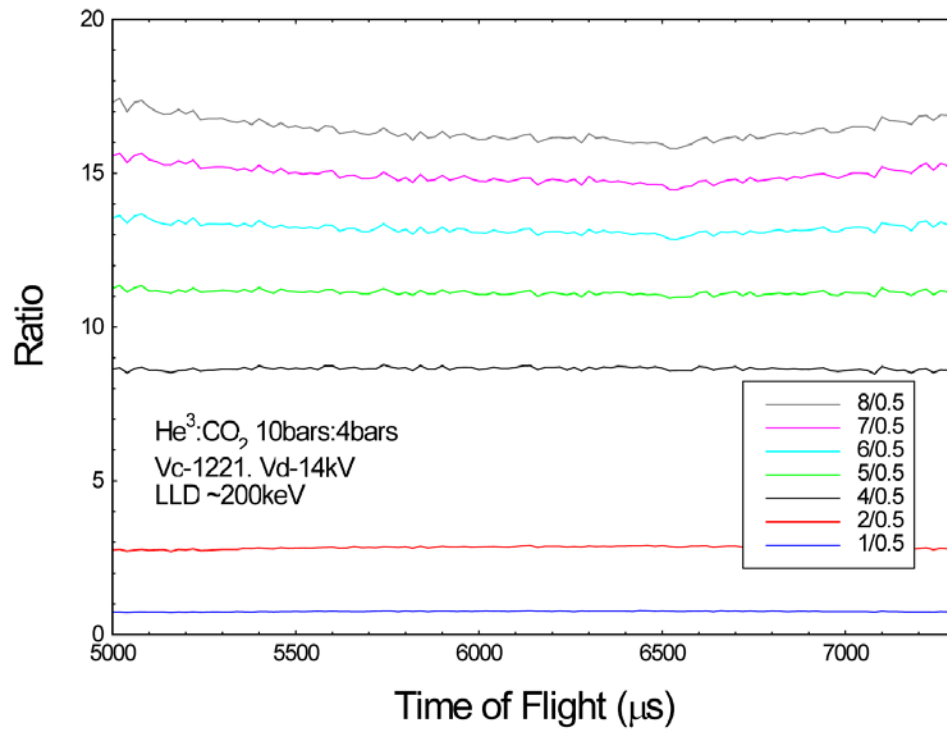
Figure 19: Normalised TOF spectra for reduced DAE time window
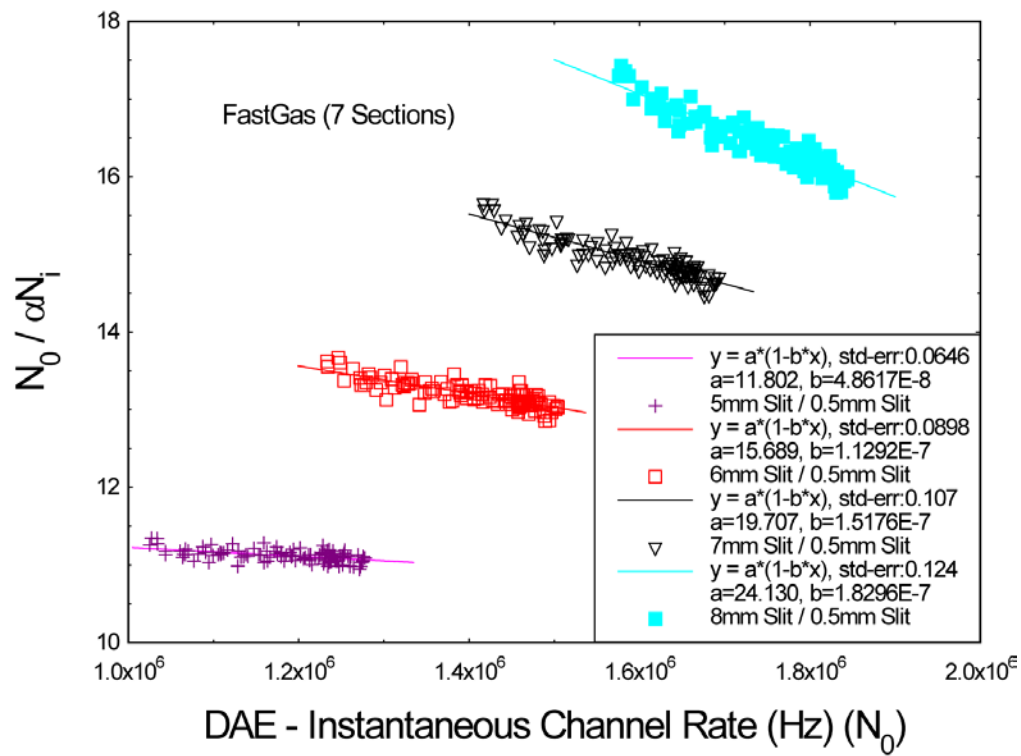

Figure 20: Deadtime Plots derived from the data of Figure 19
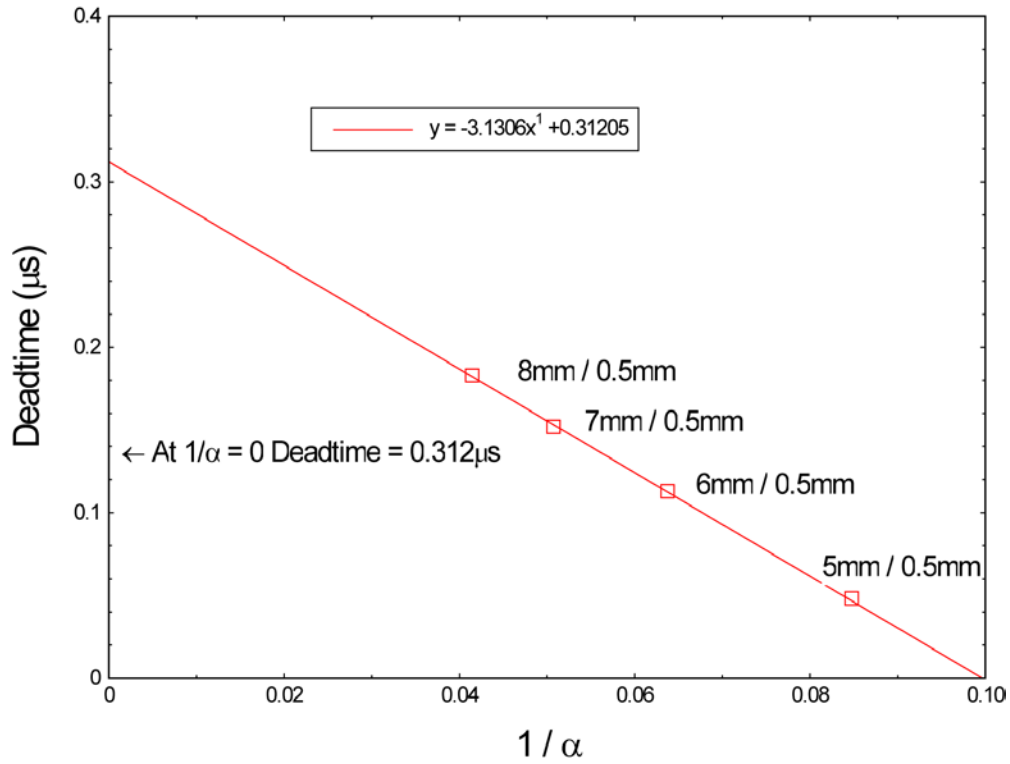
Figure 21: Asymptotic Plot estimating 7-Section Deadtime
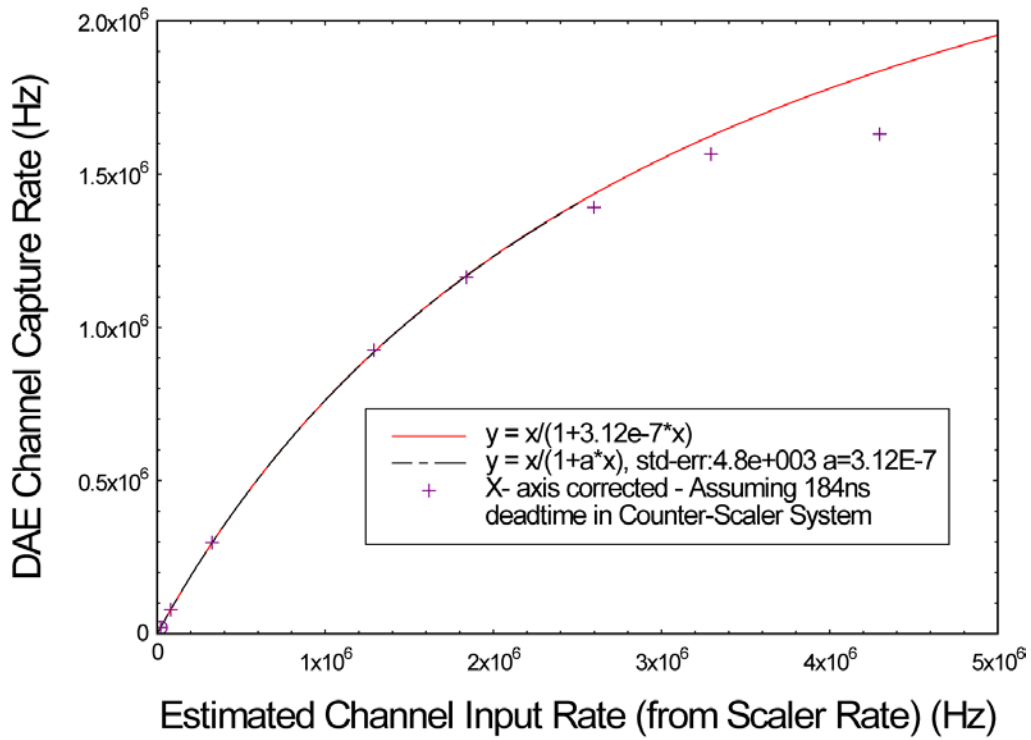
Figure 22: 7-Section Deadtime Curve (Obtained by correlating the result from Figure 21 with Scaler Data)
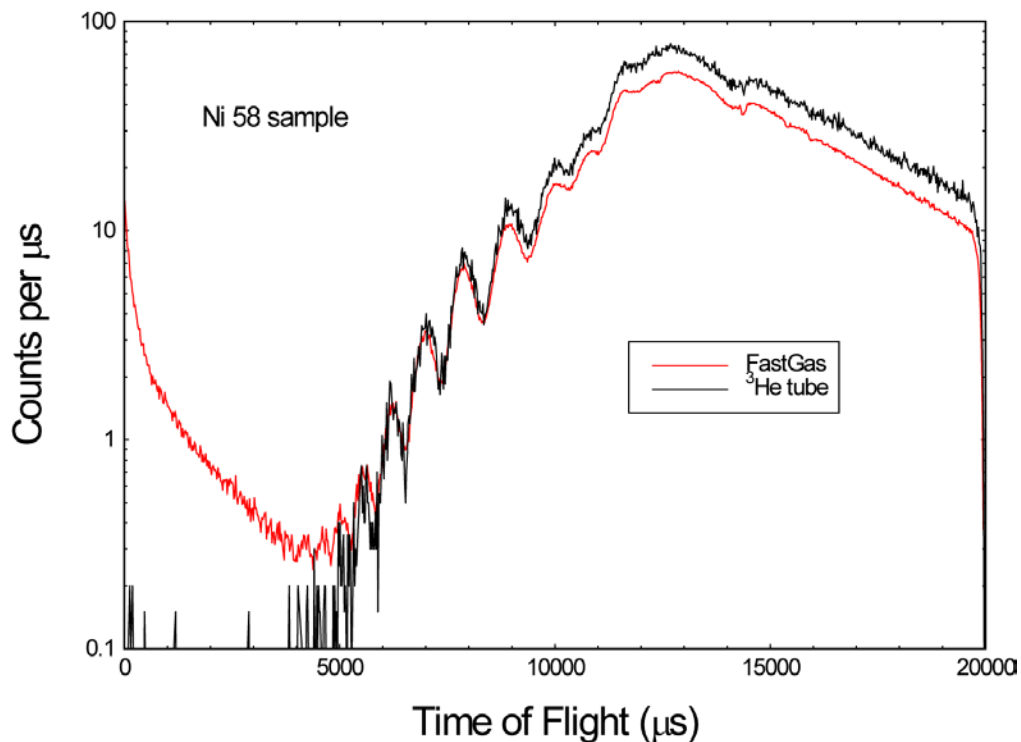
Figure 23: TOF spectra for ^{58}Ni sample from FastGas and ^{3}He tube
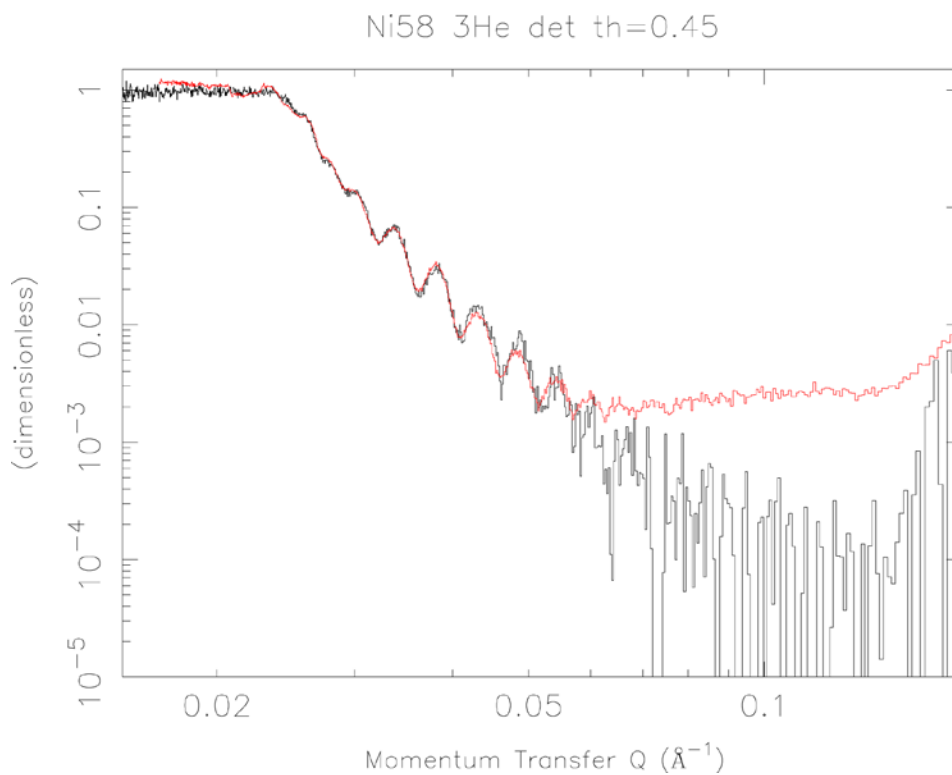
Figure 24: Reflectivity of ^{58}Ni sample as a function of momentum transfer as measured with FastGas (red curve) and the ^{3}He tube (black curve)